Rotation Detection in Light-Driven Nanorotors

P. H. Jones,[†,*] F. Palmisano,[‡] F. Bonaccorso,[§] P. G. Gucciardi,[‡] G. Calogero,[‡] A. C. Ferrari,[§] and O. M. Maragó[‡,*]

[†]Department of Physics and Astronomy, University College London, Gower Street, WC1E 6BT London, U.K., [‡]CNR-Istituto per i Processi Chimico-Fisici, Messina, Salita Sperone C. da Papardo, Faro Superiore, I-98158 Messina, Italy, and [§]Department of Engineering, University of Cambridge, Cambridge CB3 0FA, U.K.

ABSTRACT We analyze the rotational dynamics of light driven nanorotors, made of nanotube bundles and gold nanorods aggregates, with nonsymmetric shapes, trapped in optical tweezers. We identify two different regimes depending on dimensions and optical properties of the nanostructures. These correspond to alignment with either the laser propagation axis or the dominant polarization direction, or rotational motions caused by either unbalanced radiation pressure or polarization torque. By analyzing the motion correlations of the trapped nanostructures, we measure with high accuracy both the optical trapping parameters and the rotation frequency induced by the radiation pressure. Our results pave the way to improved all-optical detection, control over rotating nanomachines, and rotation detection in nano-optomechanics.

KEYWORDS: optical tweezers · nanorotors · nanotubes · gold nanoaggregates

The ability of light to exert a torque on macroscopic objects has been known since the experiments of Beth in 1936,[1] who demonstrated that polarized light transfers angular momentum to a birefringent wave plate. Since the development of optical tweezers[2] for manipulation and control of materials at the micro- and nanoscale, the need to produce controlled rotations in addition to translations has led to a number of different techniques for rotating microparticles. These include methods that rely on properties such as particle birefringence, as in Beth's original experiment,[3] form birefringence of anisotropic objects,[4,5] anisotropic scattering from the particle shape,[6−8] or transfer of optical orbital angular momentum (OAM) from a Laguerre−Gaussian beam.[9]

The development of noncontact techniques to enable the controlled manipulation, orientation, and rotation of nanoparticles and nanoaggregates is of crucial importance for their implementation as active elements in next generation nanomachines. These will require a range of components for the conversion of energy into motion. In particular, devices capable of continuous rotational motion are of critical importance for the operation of nanomachines in applications such as microscale fluid pumping in microfluidic chips.[10] Unidirectional rotational motion was previously demonstrated in systems such as catalytic microrotors[11] or molecular rotors;[12] however, the use of optical trapping methods opens the possibility of assembling and driving nanostructured components while simultaneously continually monitoring their operation and performance.

Carbon nanotubes (CNTs) are at the center of a wide range of research areas because of their unique properties that arise from their quasi-one-dimensional character.[13] They easily form ropes or bundles[14−16] due to strong van der Waals interactions;[17] thus, much effort has been made to stably disperse them in a variety of solvents[18−20] or polymers.[21,22]

Gold nanorods (AuNRs) have size-tunable optical properties, facile surface chemistry, and appropriate scale for many applications in biology and medicine.[23,24] Their potential for diagnosis and therapy stems from surface-plasmon resonance-enhanced light scattering and absorption.[25,26]

Optical trapping of nanoparticles is not straightforward. The radiation force scales with the volume of the trapped object[2] and Brownian motion[27] can easily overwhelm optical trapping;[2] indeed, optical trapping for CNTs and gold nanoparticles was demonstrated only recently.[28−37] CNT bundles usually have an almost linear geometry, with a subwavelength cross section and very high aspect ratio. Their length can be in the micrometer range, ensuring stable trapping and allowing force sensing in the femtonewton regime.[36] AuNRs exhibit strong plasmonic resonances in the near-

*Address correspondence to philip.jones@ucl.ac.uk, marago@me.cnr.it.

Received for review July 17, 2009 and accepted September 4, 2009.

Published online September 22, 2009.
10.1021/nn900818n CCC: $40.75

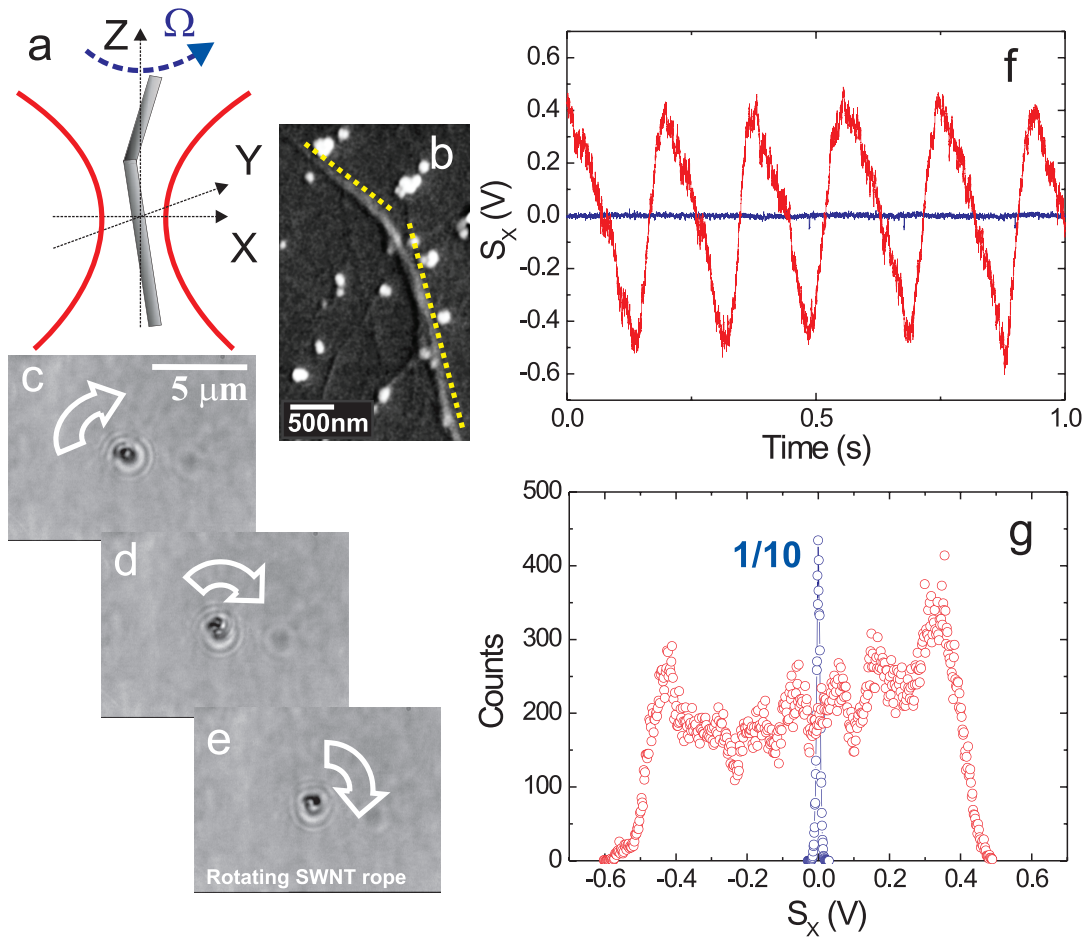

Figure 1. Optical trapping and "windmill" rotation of CNT bundles. (a) Sketch showing CNT rope geometry and orientation relative to the trap axes. (b) SEM image of an asymmetric CNT rope. (c,d,e) Sequence of video frames showing that the bundle rotates about the laser propagation axis. (f) QPD signal for the bundle projection in the *x* direction (red), which oscillates due to the rotational motion, compared to that from a symmetric bundle (blue). (g) Histogram of the QPD signal of the rotating bundle (red), compared to that of a nonrotating symmetric bundle (blue).

infrared, with high saturation intensities.[38] These resonances can be exploited to trap the AuNRs when light is tuned to the long wavelength side of the resonance.[32,35]

Here we analyze optically induced rotations of two different nanostructures manipulated by optical tweezers, where the rotation is a consequence of the particle shape: asymmetric CNT bundles and AuNR aggregates. We find that anisotropic scattering (the so-called "windmill effect" by analogy to the sails of a windmill driven into continuous rotation) causes rotation about the laser propagation direction, and form birefringence, in which an elongated nanoparticle has anisotropic polarizability, aligns the particle axis with the dominant laser polarization direction. Both effects are significant in the design of microfabricated elements for future applications in optically assembled and driven nanomachines. We then present an accurate measurement of the optical trapping and rotations of these nanoparticles, based on a correlation function analysis of the particle motion.

RESULTS AND DISCUSSION

Optical Trapping and Rotation. We consider the steady-state optically driven rotation of trapped nanoparticles, and the quantitative measurement of their rotation from the analysis of the tracking signals. We investigate two distinct nanostructures, with different geometries and light-scattering properties: bundles of single wall CNTs and AuNR aggregates, prepared as described in Methods.

Figure 1 shows optical trapping and motion detection of a CNT rope, consisting of two bundles ~1 and 2 μm long joined at one end, with their long axes making a small angle relative to each other. The transverse bundle dimension is estimated to be ~10 nm from atomic force microscopy (AFM) images.[37] Figure 1a sketches the CNT rope and its orientation in the optical tweezers, along with the coordinate system used and the direction of the optically induced rotation. Figure 1b is a scanning electron microscope (SEM) image of this rope. Figure 1 panels c and d indicate that the rope aligns parallel to the trap axis (*z*) and, as a consequence of its structure, is set into continuous rotation

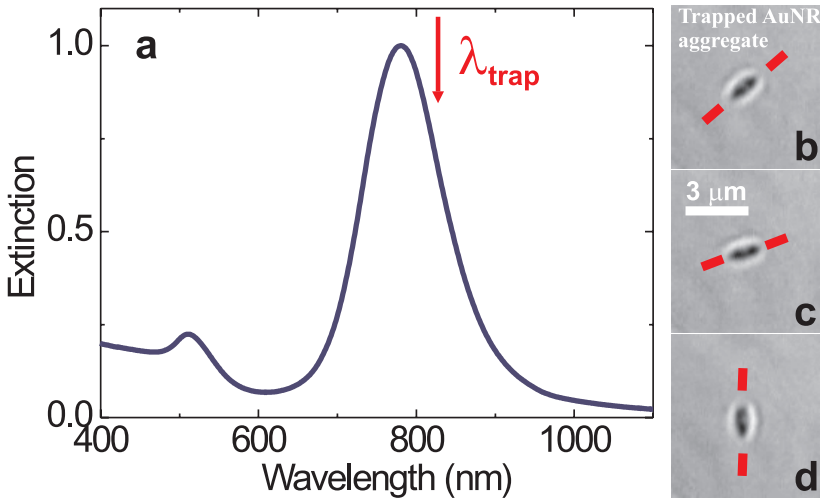

Figure 2. (a) AuNR extinction spectrum, showing the plasmon resonance. The trapping laser wavelength is indicated by a red arrow. (b,c,d) Images of an optically trapped aggregate. This aligns with the long axis parallel to the dominant polarization component in the trap and is rotated by the changing polarization direction caused by turning a half wave plate in the beam path.

about this axis, as excess radiation pressure on one side of this anisotropic object drives rotation in a similar way as the wind in a windmill[39] (see Supporting Information for a movie). This rotational motion is evident from the four-quadrant photodiode (QPD) tracking signal in Figure 1f, showing an oscillation as the projection of the CNT rope on the measurement direction changes, compared to a symmetric, nonrotating CNT bundle, which exhibits only Brownian fluctuations.[36] Figure 1g plots a histogram of the tracking signals, further illustrating the sensitivity of this method to the driven rotation: the histogram of the symmetric bundle tracking signal is Gaussian, arising from Brownian thermal fluctuations, whereas that for the rotating asymmetric one is a convolution of the Brownian fluctuations and a sinusoidal oscillation. Previous experiments[40] reported rota-

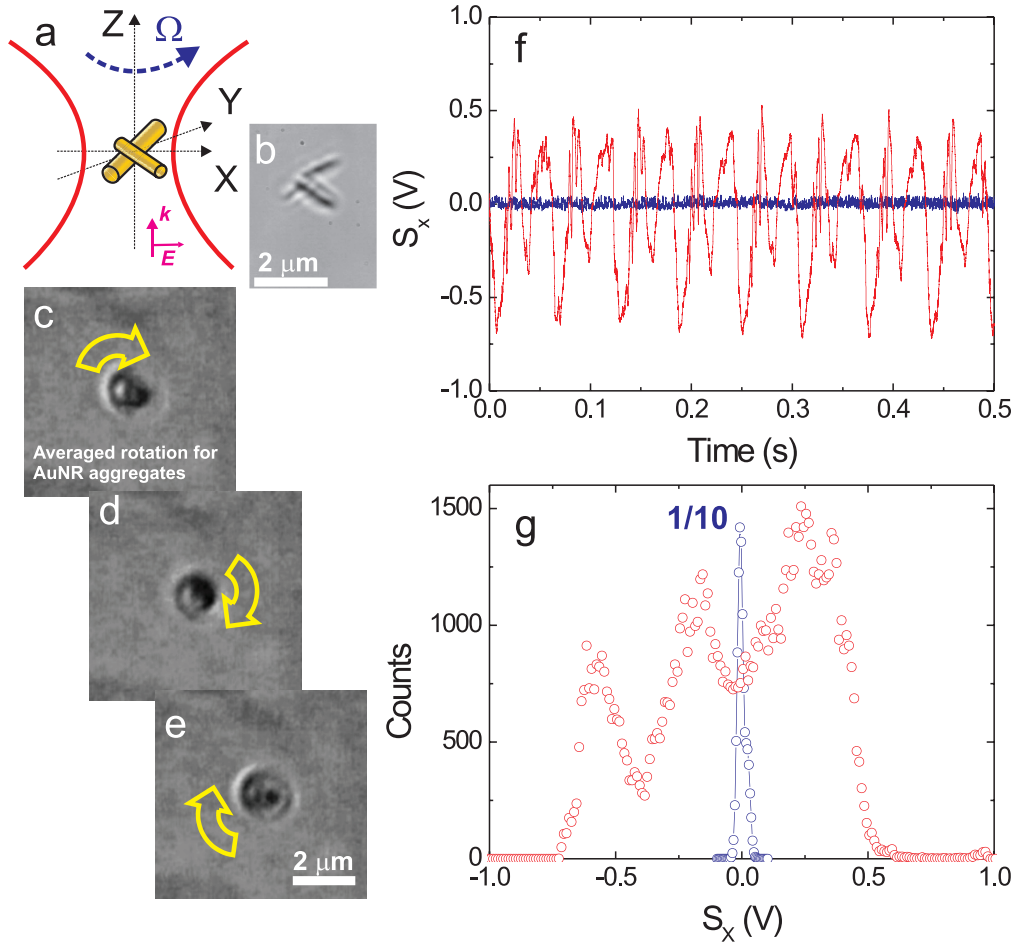

Figure 3. (a) Geometry and trapping orientation of a T-shaped AuNR aggregate. (b) SEM image. (c−e) Sequence of video frames showing the AuNR rotation. (f) Tracking signal of the projection of the aggregate onto the *x* direction (red), which oscillates as the aggregate rotates, compared to that of a single AuNR (blue). (g) Histogram of the QPD signal for the aggregate (red), showing two-frequency oscillations, compared to a Gaussian for the single AuNR (blue).

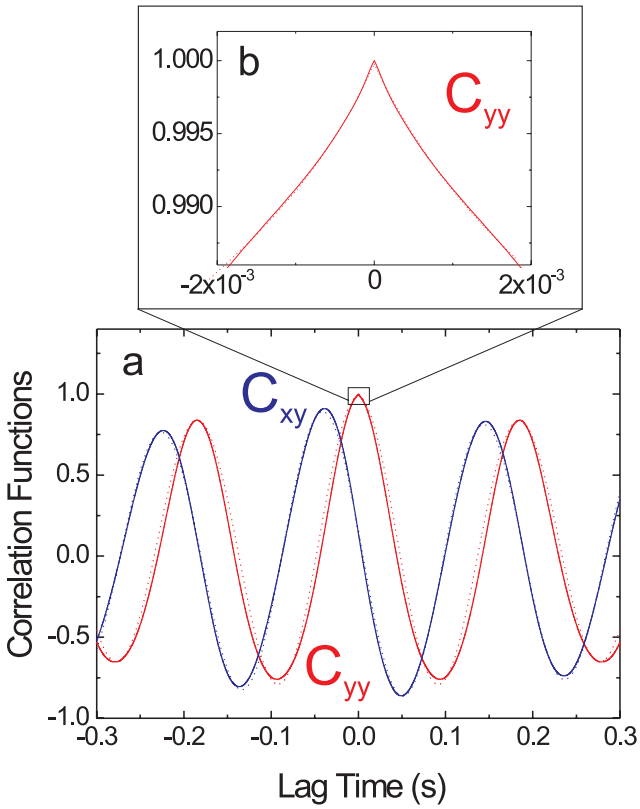

Figure 4. (a) Autocorrelation (C_{yy}) of tracking signal S_y, and cross-correlation (C_{xy}) of S_x and S_y for the asymmetric CNT bundle. Both have a sinusoidal modulation at the rotational angular frequency, Ω. (b) Expanded view of the autocorrelation signal at short lag times, showing the exponential decay characteristic of the trapping potential.

tion of CNT bundles in optical traps, as a consequence of both radiation pressure (at low optical power) and solution convection (at higher optical power). The conditions of our experiments, however, satisfy criteria set by ref 41 for which heating and convection effects are small: use of water as a solvent, trapping closer to the solvent-glass coverslip interface, and low optical trapping power (an order of magnitude less than the 100 mW indicated by ref 41 for laser-induced heating to be significant).

We compare these results with a second test object consisting of a AuNR aggregate. Since the behavior of nanostructures in an optical trap depends on their physical and optical properties, we expect the AuNR dynamics to be significantly different from that of CNTs. For one-dimensional nanostructures with transverse dimension $d \ll \lambda$, where λ is the optical trapping wavelength, the orientation in the trap depends on the particle length L, which determines the balance of optical torques that control the alignment. For dielectric particles this was shown to exhibit a critical behavior at $L = 0.36\lambda$.[42,43] Experimentally, for λ in the near-infrared, nanostructures longer than ~300 nm align with the laser propagation direction,[37,44] whereas shorter ones align transversely to the trap axis and parallel to the dominant polarization.[45]

Although the overall length of our AuNR aggregates (~2 μm) exceeds the critical value for axial alignment, the individual AuNRs are short (each being ~10 nm × 45 nm). The trapping forces and effects of polarization alignment are enhanced by the proximity of the laser wavelength to the AuNR plasmon resonance (which is 780 nm for a 10 nm × 45 nm AuNR,[32,34,35] as seen in the extinction spectrum in Figure 2a), resulting in alignment transverse to the trap axis. The trap laser polarization direction can be changed by rotating a half-wave plate in the beam path, hence, controlled rotation of an ellipsoidal AuNR aggregate is possible, as in Figure 2b,d.

Continuous rotation in the optical trap is observed for AuNR aggregates with an asymmetric morphology. We consider one with an asymmetric T-shape. Figure 3a sketches this aggregate geometry in the optical trap, and Figure 3b shows an optical image. When trapped, this object orients with its plane perpendicular to the trap axis (indicated by **k**). We contrast this with the larger polymer cross object used in ref 7. This was aligned with its plane containing the trap axis. In addition to the rotation arising from the unbalanced radiation pressure, our AuNR aggregate experiences an additional torque due to form birefringence, as it attempts to align the long axis with the laser polarization.[46] This effect is further enhanced by the AuNR plasmon resonance,[32] with the result that the structure is set it into rapid rotation, as seen in the frames of Figure 3c−e (see Supporting Information for the movie).

The particle tracking signal from one axis is plotted in Figure 3f with, for comparison, that of a single optically trapped rod. Again, the single AuNR shows only Brownian fluctuations in position, whereas the T-shaped structure exhibits a strong modulation due to rotations. The corresponding histograms are reported in Figure 3g. These are Gaussian for the single AuNR, but have a more complicated structure for the T-shaped test object. The form of the histogram is due to two frequency components present in the tracking signal. Their origin will be discussed next.

Correlation Function Analysis of Optical Rotation. Autocorrelation functions of the tracking signals are a powerful tool for characterization of optical tweezers trapping forces, yielding information about the spring constant of the trap, κ.[36,47] The center-of-mass coordinates x, y of the trapped particles (and hence the signals arising from motion in these directions, S_x, S_y) are stochastic variables. For a strongly overdamped harmonic oscillator, the autocorrelation function $C_{ii}(\tau) = \langle S_i(t)\, S_i(t+\tau)\rangle$ ($i = x, y$) yields an exponential decay with characteristic time $(\kappa\Gamma)^{-1}$, where Γ is the hydrodynamic mobility coefficient.[48] For an asymmetric particle rotating about the trap

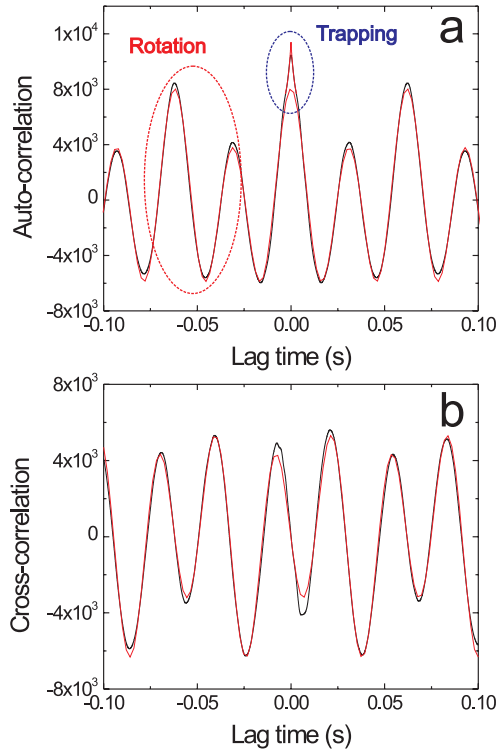

Figure 5. (a) Autocorrelation of the AuNR aggregate tracking signals (C_{xx}) showing sinusoidal modulation due to rotation, and, at short times, exponential decay due to trapping. (b) Cross-correlation (C_{xy}) showing the same two-frequency oscillation as the autocorrelation.

axis, such as our CNT rope, the tracking signals include a contribution from the projection of the particle onto the axis, which varies with particle rotation as $S_x(t) = x(t) + a\cos(\Omega t)$, $S_y(t) = y(t) + a\sin(\Omega t)$, where Ω is the rotation (angular) frequency and a is a constant dependent on the object and light scattering geometries. Here we neglect the polar and azimuthal fluctuations, because the rotation induced by the radiation pressure has a much larger amplitude, and consider motion only in the plane perpendicular to the rotation axis (xy plane). In this case we evaluate not only the autocorrelation functions, but also their cross-correlations:

$$C_{ii}(\tau) = \frac{k_B T}{\kappa_i} e^{-\omega_i \tau} + \frac{a^2}{2}\cos(\Omega\tau), \quad i = x, y \qquad (1)$$

$$C_{xy}(\tau) = \frac{a^2}{2}\sin(\Omega\tau) \qquad (2)$$

where $\omega_i = \kappa_i \Gamma$ is the relaxation frequency. As shown in Figure 4a for the asymmetric CNT bundle, both cross- and autocorrelation functions present a strong sinusoidal modulation, with the autocorrelation C_{yy} having an additional exponential decay, seen at small lag time, τ, Figure 4b. Fitting functions of the form of eqs 1, and 2 to these signals yields a rotational angular frequency for the CNT bundle $\Omega_{CNT} = 33.91 \pm 0.01$ rad s^{-1}. The relaxation frequency of

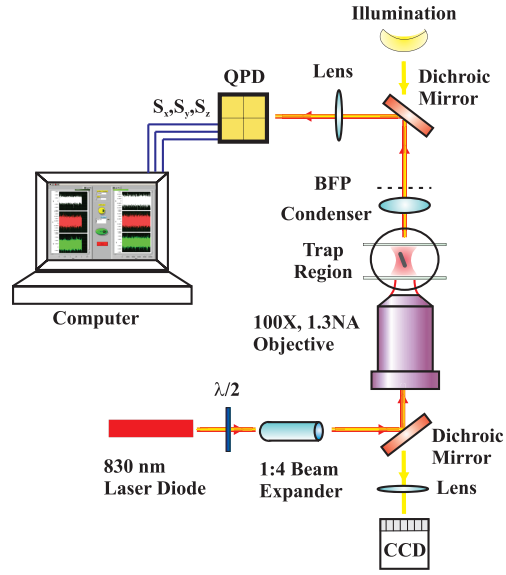

Figure 6. Diagram of experimental setup.

the exponential decay is $\omega_{CNT} = 830 \pm 20$ rad s^{-1}. From this, using the hydrodynamic mobility coefficient for a rodlike object in the direction perpendicular to its axis,[36] $\Gamma_i = \Gamma_\perp \approx 137$ μm/pNs ($i = x, y$), we obtain the trap transverse spring constant in this direction $\kappa_y \approx 6$ pN/μm.

We now explain the form of the AuNR aggregate signals by considering an asymmetric planar structure rotating in the optical trap potential about the z -axis at a frequency Ω. We can have two contributions to the interference pattern, symmetric and nonsymmetric with respect to a main axis, and rotating in the xy plane. The nonsymmetric part rotates at a frequency Ω, as discussed above for the CNT bundles, whereas the symmetric part leads to a signal modulation at a frequency 2Ω. Thus, we can write the resulting QPD signals as

$$S_x \propto x + A\cos(\Omega t) + B\cos(2\Omega t) \qquad (3)$$

$$S_y \propto y + A\sin(\Omega t) + B\sin(2\Omega t) \qquad (4)$$

where x and y are the center-of-mass coordinates, and A and B are geometrical constants.

Recalling the stochastic nature of the center-of-mass X_i coordinates, it is possible to show that the related autocorrelation functions of the QPD signals $C_{ii}(\tau) = \langle S_i(t)\, S_i(t+\tau)\rangle$ are

$$C_{xx} \propto \left[\langle x(t)\, x(t+\tau)\rangle + \frac{A^2}{2}\cos(\Omega\tau) + \frac{B^2}{2}\cos(2\Omega\tau)\right] \qquad (5)$$

$$C_{yy} \propto \left[\langle y(t)\, y(t+\tau)\rangle + \frac{A^2}{2}\cos(\Omega\tau) + \frac{B^2}{2}\cos(2\Omega\tau)\right] \qquad (6)$$

where the autocorrelations of the center-of-mass coordinates $\langle x(t)\, x(t+\tau)\rangle$ and $\langle y(t)\, y(t+\tau)\rangle$ are expo-

nentially decaying. Hence, the autocorrelations of the transverse signals now contain combined information on center-of-mass fluctuations and angular rotation, which lead to oscillations at Ω from the nonsymmetric part, and 2Ω from the symmetric part.

Similarly, the transverse signals cross-correlation $C_{xy}(\tau) = \langle S_x(t)\, S_y(t+\tau)\rangle = C_{yx}(-\tau)$ is

$$C_{xy} \propto \frac{A^2}{2}\sin(\Omega\tau) + \frac{B^2}{2}\sin(2\Omega\tau) \qquad (7)$$

As the center-of-mass coordinates x, y are uncorrelated, the transverse tracking signals cross-correlation shows only the oscillations related to optically induced rotations in quadrature with the autocorrelation.

Examples of signals auto- and cross-correlation for the AuNR aggregate are plotted in Figure 5a,b. Both graphs show the two-frequency sinusoidal oscillation expected from the analysis above. A fit with functions of the form of eqs 6 and 7 yields a rotation frequency $\Omega_{AuNR} = 101.6 \pm 0.1$ rad s^{-1}. In addition, the autocorrelation has an exponential decay in the region of $\tau = 0$, with a relaxation frequency $\omega_{AuNR} = 476 \pm 5$ rad s^{-1}.

CONCLUSIONS

We have demonstrated that optical tweezers can be used to trap a variety of nanomaterials, whose subsequent dynamics depends on their morphology and optical properties. In particular we have studied self-assembled nanoaggregates whose shape gives rise to continuous rotation in the optical tweezers. Trapping, rotation, and motion detection were performed simultaneously with a single laser beam using the methods of back focal plane interferometry for particle tracking. A correlation function analysis of the tracking signals allowed us to quantify the optical trapping parameters and speed of rotation. This method is universal and can be applied to particles of arbitrary shape, as considered theoretically in ref 46, or for microfabricated elements.[6] We expect our results to enable real-time monitoring and control of optically assembled and light-driven nanomachines by all-optical methods, thus taking a significant step toward the integration of such systems into, for example, lab-on-a-chip devices, where trapped nanostructures may act as rotational probes or as light-driven nanopumps.

METHODS

Our experimental setup for optical trapping is sketched in Figure 6. It consists of optical tweezers constructed around an inverted microscope, equipped with an Olympus Uplan FLN × 100 NA 1.3 objective, which serves to both tightly focus the laser beam for optical trapping, and image the trapped particles. The laser source is an infrared laser diode, with $\lambda = 830$ nm and maximum output power 150mW. Its beam is circularized using an anamorphic prism pair. Due to losses in the optical path, the maximum power in the sample plane is ~15mW. The apparatus also includes a half-wave plate to set the direction of linear polarization. Particle motion in the optical tweezers is detected by means of back focal plane (BFP) interferometry,[49] whereby the interference pattern between forward scattered and unscattered light in the back aperture of the microscope condenser is imaged onto a four-quadrant photodiode (QPD). The outputs Q_i from all quadrants are processed through an analog circuit board that generates electrical signals proportional to the trapped particle's displacement in the three directions (particle tracking). In the system shown in Figure 6 the signal $S_x = (Q_1 + Q_3) - (Q_2 + Q_4)$ is proportional to the displacement in the x direction, while $S_y = (Q_1 + Q_2) - (Q_3 + Q_4)$ is proportional to that in the y direction, and the four-quadrant sum $S_z = (Q1 + Q2 + Q3 + Q4)$ is proportional to the displacement in the z direction. The analysis of these signals gives a wealth of information on the calibration of the trapping potential, on the measure of spring constants, on microrheology, and, more generally, on Brownian motion spectroscopy.

Nanotube samples are prepared using purified HiPCO single wall CNTs (Carbon Nanotechnology, Inc.) dispersed in water with the aid of sodium dodecyl benzene sulfonate (SDBS), a linear chain surfactant containing a flexible cylindrical body.[19,50] SDBS, as many other linear chain surfactants, forms spherical or ellipsoidal micelles in aqueous solution.[51,52] A ~0.2 mg/mL portion of CNT dispersion is added to 10 mL of deionized water with 0.2% w/v surfactant. The suspensions are then ultrasonically treated in a 200 W, 20 kHz sonicator bath (Nanoruptor, Diagenode) for 2 h. After ultrasonication, the insoluble materials (*e.g.*, catalysts, amorphous carbon, large CNT bundles) are removed by vacuum filtration using 0.7 μm pore size filters.[53] The presence of small bundles is monitored by photoluminescence excitation spectroscopy.[16]

The AuNR aggregate solutions are purchased from Nanopartz, Salt Lake City. These are composed of 10 nm × 45 nm AuNRs dispersed in water with <0.1% ascorbic acid and <0.1% cetyl trimethylammonium bromide (CTAB) capping agent. The extinction spectrum, shown in Figure 2a, is recorded on a Perkin-Elmer L20 spectrophotometer UV−vis−NIR and reveals a plasmon wavelength of 780 nm.

A few tens of microliters of each nanoparticle solution (CNT bundles or AuNR aggregates) is then placed in a 100 mm^3 chamber attached to a piezo-stage with 1 nm resolution. The stage is used to steer nanoparticles close to the diffraction-limited laser beam waist where they are trapped and set into rotation.

Owing to the high rotation frequency of our light-driven nanorotors, video microscopy is not suitable for measuring the rotation speed, as only an average image over the exposure time of each frame is recorded. We therefore use a method based on recording an interferometric particle tracking signal and evaluating the correlations between the motion in orthogonal directions.[54] The frequency response of this technique is limited by the bandwidth of the electronics that records the tracking signal (~100 kHz in our experiment), therefore enabling detection of much higher rotational frequencies. Furthermore, the same laser beam that drives the nanoparticles' rotation is also used for the detection of that motion, thus considerably simplifying the experimental geometry.

Acknowledgment. We thank the Royal Society and British Council for financial support. A.C.F. acknowledges funding from the European Research Council Grant NANOPOTS. F.B. acknowledges funding from a Newton International Fellowship.

Supporting Information Available: Movie showing optical rotation of SWNT rope; movie showing optical rotation of AuNR aggregate. This material is available free of charge *via* the Internet at http://pubs.acs.org.

REFERENCES AND NOTES

1. Beth, R. Mechanical Detection and Measurement of the Angular Momentum of Light. *Phys. Rev.* **1936**, *50*, 115–125.
2. Ashkin, A.; Dziedzic, J. M.; Bjorkholm, J. E.; Chu, S. Observation of a Single-Beam Gradient Force Optical Trap for Dielectric Particles. *Opt. Lett.* **1986**, *11*, 288–290.
3. Friese, M. E. J.; Nieminen, T. A.; Heckenberg, N. R.; Rubinsztein-Dunlop, H. Optical Alignment and Spinning of Laser-Trapped Microscopic Particles. *Nature* **1998**, *394*, 348–350.
4. Bishop, A. I.; Nieminen, T. A.; Heckenberg, N. R.; Rubinsztein-Dunlop, H. Optical Application and Measurement of Torque on Microparticles of Isotropic Nonabsorbing Material. *Phys. Rev. A* **2003**, *68*, 033802.
5. La Porta, A.; Wang, M. D. Optical Torque Wrench: Angular Trapping, Rotation, and Torque Detection of Quartz Microparticles. *Phys. Rev. Lett.* **2004**, *92*, 190801.
6. Galajda, P.; Ormos, P. Complex Micromachines Produced and Driven by Light. *Appl. Phys. Lett.* **2001**, *78*, 249–251.
7. Galajda, P.; Ormos, P. Orientation of Flat Particles in Optical Tweezers by Linearly Polarized Light. *Opt. Express* **2003**, *11*, 446–451.
8. Khan, M.; Sood, A. K.; Deepak, F. L.; Rao, C. N. R. Nanorotors Using Asymmetric Inorganic Nanorods in an Optical Trap. *Nanotechnology* **2006**, *17*, S287–S290.
9. Friese, M. E. J.; Enger, J.; Rubinsztein-Dunlop, H.; Heckenberg, N. R. Optical Angular-Momentum Transfer to Trapped Absorbing Particles. *Phys. Rev. A* **1996**, *54*, 1593–1596.
10. Maruo, S.; Inoue, H. Optically Driven Micropump Produced by Three-Dimensional Two-Photon Microfabrication. *Appl. Phys. Lett* **2006**, *89*, 144101-1–144101-3.
11. Wang, Y.; Fei, S.; Byun, Y.-M.; Lammert, P. E.; Crespi, V. H.; Sen, A.; Mallouk, T. E. Dynamic Interactions Between Fast Microscale Rotors. *J. Am. Chem. Soc.* **2009**, *131*, 9926–9927.
12. Koumura, N.; Zijlstra, R. W. J.; van Delden, R. A.; Harada, N.; Feringa, B. L. Light-Driven Monodirectional Molecular Rotor. *Nature* **1999**, *401*, 152–155.
13. Jorio, A., Dresselhaus, G., Dresselhaus, M. S., Eds. *Carbon Nanotubes*; Springer-Verlag: Berlin, Heidelberg, 2008.
14. Thess, A.; Lee, R.; Nikolaev, P.; Dai, H.; Petit, P.; Robert, J.; Xu, C.; Lee, Y. H.; Kim, S. G.; Rinzler, A. G.; *et al.* Crystalline Ropes of Metallic Carbon Nanotubes. *Science* **1996**, *273*, 483–487.
15. Journet, C.; Maser, W. K.; Bernier, P.; Loiseau, A.; Lamy de la Chapelle, M.; Lefrant, S.; Deniard, P.; Lee, R.; Fisher, J. E. Large-Scale Production of Single-Walled Carbon Nanotubes by the Electric-Arc Technique. *Nature* **1997**, *388*, 756–758.
16. Tan, P. H.; Rozhin, A. G.; Hasan, T.; Hu, P.; Scardaci, V.; Milne, W. I.; Ferrari, A. C. Photoluminescence Spectroscopy of Carbon Nanotube Bundles: Evidence for Exciton Energy Transfer. *Phys. Rev. Lett.* **2007**, *99*, 137402-1–137402-4.
17. Hertel, T.; Walkup, R. E.; Avouris, P. Deformation of Carbon Nanotubes by Surface Van der Waals Forces. *Phys. Rev. B* **1998**, *58*, 13870–13873.
18. O'Connell, M. J.; Bachilo, S. M.; Huffman, C. B.; Moore, V. C.; Strano, M. S.; Haroz, E. H.; Rialon, K. L.; Boul, P. J.; Noon, W. H.; Kittrell, C.; *et al.* Band Gap Fluorescence from Individual Single-Walled Carbon Nanotubes. *Science* **2002**, *297*, 593–596.
19. Moore, V. C.; Strano, M. S.; Haroz, E. H.; Hauge, R. H.; Smalley, R. E.; Schmidt, J.; Talmon, Y. Individually Suspended Single-Walled Nanotubes in Various Surfactants. *Nano Lett.* **2003**, *3*, 1379–1382.
20. Zheng, M.; Jagota, A.; Semke, E. D.; Diner, B. A.; Mclean, R. S.; Lustig, S. R.; Richardson, R. E.; Tassi, N. G. DNA-Assisted Dispersion and Separation of Carbon Nanotubes. *Nat. Mater.* **2003**, *2*, 338–342.
21. Hasan, T.; Scardaci, V.; Tan, P. H.; Rozhin, A. G.; Milne, W. I.; Ferrari, A. C. Stabilization and "Debundling" of Single-Wall Carbon Nanotube Dispersions in *N*-Methyl-2-Pyrrolidone (NMP) by Polyvinylpyrrolidone (PVP). *J. Phys. Chem. C* **2007**, *111*, 12594–12602.
22. Hasan, T.; Tan, P. H.; Bonaccorso, F.; Rozhin, A. G.; Scardaci, V.; Milne, W. I.; Ferrari, A. C. Polymer-Assisted Isolation of Single Wall Carbon Nanotubes in Organic Solvents for Optical-Quality Nanotube Polymer Composites. *J. Phys. Chem. C* **2008**, *112*, 20227–20232.
23. Salata, O. V. Applications of Nanoparticles in Biology and Medicine. *J. Nanobiotechnol.* **2004**, *2*, 3.
24. Kneipp, J. H.; Kneipp, H.; McLaughlin, M.; Brown, D.; Kneipp, K. *In Vivo* Molecular Probing of Cellular Compartments with Gold Nanoparticles and Nanoaggregates. *Nano Lett.* **2006**, *6*, 2225–2231.
25. Kneipp, K.; Kneipp, H.; Kneipp, I.; Dasari, R. R.; Feld, M. S. Surface-Enhanced Raman Scattering and Biophysics. *J. Phys.: Condens. Matter* **2002**, *14*, R597–R624.
26. El-Sayed, I.; Huang, X.; El-Sayed, M. Selective Laser Photo-Thermal Therapy of Epithelial Carcinoma Using Anti-EGFR Antibody Conjugated Gold Nanoparticles. *Cancer Lett.* **2005**, *239*, 129–135.
27. Einstein, A. Über die von der Molekularkinetischen Theorie der Wärme Geforderte Bewegung von in Ruhenden Flüssigkeiten Suspendierten Teilchen. *Ann. Phys.* **1905**, *17*, 549–560.
28. Tan, S.; Lopez, H A.; Cai, C. W.; Zhang, Y. Optical Trapping of Single-Walled Carbon Nanotubes. *Nano Lett.* **2004**, *4*, 1415–1419.
29. Plewa, J.; Tanner, E.; Mueth, D.; Grier, D. Processing Carbon Nanotubes with Holographic Optical Tweezers. *Opt. Express* **2004**, *12*, 1978–1981.
30. Zhang, J.; Kim, H. I.; Oh, C. H.; Sun, X.; Lee, H. Multidimensional Manipulation of Carbon Nanotube Bundles with Optical Tweezers. *Appl. Phys. Lett.* **2006**, *88*, 053123-1–053123-3.
31. Hansen, P. M.; Bhatia, V. K.; Harrit, N.; Oddershede, L. Expanding the Optical Trapping Range of Gold Nanoparticles. *Nano Lett.* **2005**, *5*, 1937–1942.
32. Pelton, M.; Liu, M.; Kim, H. Y.; Smith, G.; Guyot-Sionnest, P.; Scherer, N. F. Optical Trapping and Alignment of Single Gold Nanorods by Using Plasmon Resonances. *Opt. Lett.* **2006**, *31*, 2075–2077.
33. Seol, Y.; Carpenter, A. E.; Perkins, T. T. Gold Nanoparticles: Enhanced Optical Trapping and Sensitivity Coupled with Significant Heating. *Opt. Lett.* **2006**, 2429–31.
34. Toussaint, K. C.; Liu, M.; Pelton, M.; Pesic, J.; Guffey, M. J.; Guyot-Sionnest, P.; Scherer, N. F. Plasmon Resonance-Based Optical Trapping of Single and Multiple Au Nanoparticles. *Opt. Express* **2007**, *15*, 12017–12029.
35. Selhuber-Unkel, C.; Zins, I.; Schubert, O.; Sönnichsen, C.; Oddershedde, L. B. Quantitative Optical Trapping of Single Gold Nanorods. *Nano Lett.* **2008**, *8*, 2998–3003.
36. Marago, O. M.; Jones, P. H.; Bonaccorso, F.; Scardaci, V.; Gucciardi, P. G.; Rozhin, A.; Ferrari, A. C. Femtonewton Force Sensing with Optically Trapped Nanotubes. *Nano Lett.* **2008**, *8*, 3211–3216.
37. Marago, O. M.; Gucciardi, P. G.; Bonaccorso, F.; Calogero, G.; Scardaci, V.; Rozhin, A.; Ferrari, A. C.; Jones, P. H.; Saija, R.; Borghese, F.; *et al.* Optical Trapping of Carbon Nanotubes. *Phys. E* **2008**, *8*, 2347–2351.
38. Novotny, L.; Hecht, B. *Principles of Nano-Optics;* Cambridge University Press: Cambridge, U.K., 2006.
39. Higurashi, E.; Ukita, H.; Tanaka, H.; Ohguchi, O. Optically Induced Rotation of Anisotropic Micro-objects Fabricated by Surface Micromachining. *Appl. Phys. Lett.* **1994**, *64*, 2209–2210.
40. Zhang, J.; Kim, T. G.; Jeoung, S. C.; Yao, F.; Lee, H.; Sun, X. Controlled Trapping and Rotation of Carbon Nanotube Bundle with Optical Tweezers. *Opt. Commun.* **2006**, *267*, 260–263.
41. Peterman, E. G. J.; Gittes, F.; Schmidt, C. F. Laser-Induced Heating in Optical Traps. *Biophys. J.* **2003**, *84*, 1308–1316.
42. Rockstuhl, C.; Herzig, H. P. Calculation of the Torque on Dielectric Elliptical Cylinders. *J. Opt. Soc. Am., A* **2005**, *22*, 109–116.
43. Borghese, F.; Denti, P.; Saija, R.; Iati, M. A.; Marago, O. M. Radiation Torque and Force on Optically Trapped Linear Nanostructures. *Phys. Rev. Lett.* **2008**, *100*, 163903-1–163903-4.
44. Nakayama, Y.; Pauzauskie, P.; Radenovic, A.; Onorato, R.; Saykally, R.; Liphardt, J.; Yang, P. Tunable Nanowire Nonlinear Optical Probe. *Nature* **2007**, *447*, 1098–1101.

45. Bonin, K.; Kourmanov, B.; Walker, T. Light Torque Nanocontrol, Nanomotors and Nanorockers. *Opt. Express* **2002**, *10*, 984–989.
46. Simpson, S. H.; Benito, D. C.; Hanna, S. Polarization-Induced Torque in Optical Traps. *Phys. Rev. A* **2007**, *76*, 043408-1−043408-14.
47. Meiners, J.-C.; Quake, S. R. Direct Measurement of Hydrodynamic Cross Correlations Between Two Particles in an External Potential. *Phys. Rev. Lett.* **1999**, *82*, 2211–2214.
48. Happel, J.; Brenner, H. *Low Reynolds Number Hydrodynamics*; Springer: Berlin, 1981.
49. Gittes, F.; Schmidt, C. Interference Model for Back-Focal-Plane Displacement Detection in Optical Tweezers. *Opt. Lett.* **1998**, *23*, 7–9.
50. Islam, M. F.; Rojas, E.; Bergey, D. M.; Johnson, A. T.; Yodh, A. G. High Weight Fraction Surfactant Solubilization of Single-Wall Carbon Nanotubes in Water. *Nano Lett.* **2003**, *3*, 269–273.
51. Romanini, D.; Avalle, G.; Farruggia, B.; Nerli, B.; Pico, G. Spectroscopy Features of the Binding of Polyene Antibiotics to Human Serum Albumin. *Chem. Biol. Interact.* **1998**, *115*, 247–260.
52. Calafato, N. R.; Pico, G. Griseofulvin and Ketoconazole Aolubilization by Bile Salts Studied Using Fluorescence Spectroscopy. *Colloid Surf., B* **2006**, *47*, 198–204.
53. Scardaci, V.; Sun, Z.; Wang, F.; Rozhin, A. G.; Hasan, T.; Hennrich, F.; White, I. H.; Milne, W. I.; Ferrari, A. C. Carbon Nanotube Polycarbonate Composites for Ultrafast Lasers. *Adv. Mater.* **2008**, *20*, 4040–4043.
54. Volpe, G.; Petrov, D. Torque Detection Using Brownian Fluctuations. *Phys. Rev. Lett.* **2006**, *97*, 210603-1–210603-4.